atmosphere

MDPI

Article

Changes in the Seasonal Cycle of Heatwaves, Dry and Wet Spells over West Africa Using CORDEX Simulations

Assi Louis Martial Yapo [1,2,*], Benjamin Komenan Kouassi [2,3], Adama Diawara [2,3], Fidèle Yoroba [2,3], Adjoua Moise Landry Famien [1], Pêlèmayo Raoul Touré [1], Kouakou Kouadio [2,3], Dro Touré Tiemoko [2,4], Mouhamadou Bamba Sylla [5] and Arona Diedhiou [6]

1 Department of Sciences and Technology, University Alassane Ouattara, Bouaké 01 BP V 108, Côte d'Ivoire; famien.landry@uao.edu.ci (A.M.L.F.); pelemayo@uao.edu.ci (P.R.T.)
2 Geophysical Station of Lamto (GSL), N'douci BP 31, Côte d'Ivoire; benjamin.kouassi@gmail.com (B.K.K.); diawara_adama@yahoo.fr (A.D.); fidele.yoroba49@ufhb.edu.ci (F.Y.); kk.kouadio@gmail.com (K.K.); ttouredro017@gmail.com (D.T.T.)
3 Laboratory of Sciences Matter, Environment and Solar Energy (LASMES), University Félix Houphouët-Boigny, Abidjan 22 BP 582, Côte d'Ivoire
4 Laboratory of Fundamental and Applied Physics, University Nangui Abrogoua, Abidjan 02 BP 801, Côte d'Ivoire
5 African Institute for Mathematical Sciences (AIMS), AIMS Rwanda Center, KN 3, Kigali P.O. Box 71 50, Rwanda; syllabamba@yahoo.fr
6 African Centre of Excellence on Climate Change, Biodiversity and Sustainable Agriculture (ACE CCBAD), University Félix Houphouet-Boigny, Abidjan 22 BP 582, Côte d'Ivoire; arona.diedhiou@ird.fr
* Correspondence: louismartialyapo@gmail.com or martial_yapo@uao.edu.ci

Abstract: This study analyzes the potential response of the seasonal cycle of heatwaves (HWDI) and dry (CDD) and wet (CWD) spell indices over West Africa for the near- (2031–2060) and the far-future periods (2071–2100) under RCP4.5 and RCP8.5 scenarios using Coordinated Regional Climate Downscaling Experiment (CORDEX) simulations. Despite the fact that some relative biases (an underestimation of 30% for CDD, an overestimation of about 60% for CWD, and an overestimation of about 50% for HWDI) exist, during the historical period (1976–2005) in general, the CORDEX simulations and their ensemble mean outperform the seasonal variability in the above-mentioned indices over three defined subregions of West Africa (i.e., the Gulf of Guinea and Western and Eastern Sahel). They show high correlation coefficients (0.9 in general) and less RMSE. They project an increase (about 10 and 20 days) in heatwave days for both the near- and far-future periods over the whole West African region under both RCP scenarios. In addition, projections indicate that the Sahel regions will experience a decrease (about 5 days) in wet spell days from March to November, while in the Gulf of Guinea, a decrease (about 3 days) is projected throughout the year, except in the CCCLM simulation, which indicates an increase (about 5 days) during the retreat phase of the monsoon (October to December). Our results also highlight an increase (about 80%) in dry spells over the Sahel regions that are more pronounced during the March–November period, while over the Gulf of Guinea, an increase (about 40%) is projected over the entire year. Moreover, the months of increasing dry spells and decreasing wet spells coincide, suggesting that countries in these regions could be simultaneously exposed to dry seasons associated with a high risk of drought and heatwaves under future climate conditions.

Keywords: climate change; climate extremes; RCP4.5; RCP8.5; forcing scenarios; regional climate model

Citation: Yapo, A.L.M.; Kouassi, B.K.; Diawara, A.; Yoroba, F.; Famien, A.M.L.; Touré, P.R.; Kouadio, K.; Tiemoko, D.T.; Sylla, M.B.; Diedhiou, A. Changes in the Seasonal Cycle of Heatwaves, Dry and Wet Spells over West Africa Using CORDEX Simulations. *Atmosphere* **2023**, *14*, 1582. https://doi.org/10.3390/atmos14101582

Academic Editors: Xianxiang Li and Lup Wai Chew

Received: 19 July 2023
Revised: 17 August 2023
Accepted: 28 August 2023
Published: 19 October 2023

1. Introduction

West Africa is one of the regions mostly affected by the effects of climate change due to its vulnerability, poor economy, and low capacity for adaptation [1–3]. Consequently, climate change has some societal impacts in many areas including agriculture, transportation, infrastructure, tourism, and economy [4–7]. The global temperature increase as a

result of anthropogenic climate change is one of the main drivers of the weather, thus impacting the gross domestic product (GDP). The authors of [4] showed that the least developed and developing countries are the most affected by high temperatures compared to developed countries. In addition, they also revealed that weather impacts per-capita GDP growth through all its factors of production, with the largest impacts being on total factor productivity. Beyond the connection between weather and the above sectors, human civilization evolution is also impacted by short-term adverse weather conditions [5,8]. The Intergovernmental Panel on Climate Change (IPCC)'s framework recommendations highlight that governments, nongovernmental organizations (NGOs), and stakeholders must take appropriate actions to reduce greenhouse gas emissions in order to minimize their effects in response to global warming. Moreover, climate change has enhanced the occurrence of climate extremes, including heatwaves and dry and wet spells, considered among the most dangerous hazards as they have drastic impacts on human and natural ecosystems as well as on anthropogenic activities, like infrastructures and the economy [4]. For instance, exceptional or abnormal temperature values recorded over a region or area during at least three consecutive days can cause exposure to a long dry spell, which can cause a risk of drought. However, the same region can experience wet spells, which lead to flooding. Therefore, sectors including human health, agriculture, livestock, and the environment are the most vulnerable to such risks. For example, in the tourism sector, there is an alteration of human behavior and desires due to atmospheric thermal conditions [6].

Several studies have revealed the drawback of heatwaves worldwide, particularly in Asia [9], in the Middle East [10], in America [11,12], in Europe [13–15], in France [16,17], in Russia [13,18], in Africa [19,20], and in West Africa [21–23]. These investigations have shed light on important damage, losses of life, and downturns in economies, as highlighted by [24]. Heatwaves are also exceptional events associated with a mean temperature increase and its variability [25] as well as the influence of large-scale atmospheric circulation. Unfortunately, heatwaves, dry and wet spells, and climate extremes (i.e., flooding, warm spell days, very warm day frequency, and warm night frequency) are projected to increase in intensity, duration, and frequency worldwide [26,27] and, to some extent, with different magnitudes or intensity from one area to another [28] in the context of global warming.

Heatwaves are generally lethal phenomena, but when combined with the effects of humidity, they become a serious threat [29–31]. Heatwaves can also be modulated by sea surface temperature (SST) anomalies, which can remotely influence summer heatwave variabilities over land by generating severe convection and triggering atmospheric teleconnections [32]. In the same vein, [30] underlined that hot and humid conditions prevailing in coastal regions can be more dangerous than equivalently hot but dry conditions [33]. Consequently, heatwaves can be classified into two categories: wet heatwaves, which are the most dangerous for human health, and humid heatwaves [29,30,33]. Furthermore, [34] also defined heatwaves based on the 95th percentile of the local temperature probability density function and additional criteria, including spatial and temporal extensions in Europe. They concluded that heatwaves can be classified into six classes (Russian, West European, East European, Iberian, Scandinavian, and North Sea) based on cluster analysis and several classes related to different physical mechanisms over Europe.

Thus, heatwaves are generally defined as consecutive days of extremely hot temperatures that exceed temperature thresholds [9,31]. However, this definition is not universal because a heatwave is defined based on several factors including the research application or activity sectors (health, infrastructure, and agriculture), the geographic and climatic conditions, and the thresholds [24,34].

Hence, heatwaves do not have a unique definition and occur during a certain period of at least three or six consecutive days; no study on them is documented over the West African region. Moreover, studies related to heatwaves have not analyzed the composite effects between heatwaves and other climate extremes. This study aims to provide a comprehensive analysis of heatwaves and wet and dry spells over West Africa. To this end, this work aims to evaluate the strength of the CORDEX simulations and their ensemble mean in

capturing the seasonal cycle of heatwaves and wet and dry spells under the present climate (1976–2005) conditions, with the observations from the Climate Prediction Center (CPC) as a reference, and then analyzes the projected changes in their seasonal cycles over two future periods (2031–2060 and 2071–2100) with respect to the present climate, using CORDEX simulations and their ensemble mean. In fact, CORDEX simulations were mainly used in many studies conducted over West Africa for a validation of the mean climate state, its variability, and extreme events [35–40], as well as to better understand relevant regional/local climate phenomena and their variability and changes through downscaling [41]. This study aims to provide information about the future climate changes under different Representative Concentration Pathways (RCPs) and global warming levels [23,42–47]. The RCPs are a set of scenarios containing emission, concentration, and land use trajectories based on radiative forcing in w/m^2 [48,49]. RCP4.5 and RCP8.5, referring to a radiative forcing of 4.5 w/m^2 (stabilization scenario) and a radiative forcing of 8.5 w/m^2 (high-emission scenario), respectively, are used in this study. The paper is organized as follows. First, we describe the materials and methods in Section 2. This part includes detailed information about the study domain, data, and methods, with a brief description of the defined Expert Team on Climate Change Detection and Indices (ETCCDI) indices related to heatwaves and wet and dry spells. Section 3 is the results and discussion, which is followed by the summary and conclusions in Section 4.

2. Materials and Methods

2.1. Study Domain

This study was conducted over West Africa, covering the domain (5°–15° N, 15° W–15° E) and spanning the Atlantic coast to Chad and the Gulf of Guinea to the southern fringes of the Sahara [33]. This domain is subdivided into three subregions, coherent with [35] the Western Sahel and the Eastern Sahel, located in the Sahel area and the Gulf of Guinea on the border of the Atlantic Ocean (refer to Figure 1). The identification of these subregions is based on their location, the climate variability, and other physical features including the ecosystem, the elevation, and the soil occupation. The West African region exhibits high climate variability at regional and local scales [50]. This climate is mostly influenced by the West African monsoon flux, which governs the rainy season and thus the rain-fed agriculture [50]. This region has a semi-arid and hot climate with a dry season, corresponding to an alternation between a short wet season and a very long dry season [33]. It is important to indicate that the Sahelian subregions (e.g., the Western and Eastern Sahel) have a unimodal rainfall regime, while the Gulf of Guinea region is characterized by a bimodal regime [51]. The unimodal rainfall regime of the Sahelian zone is centered around the month of August, with an annual rainfall amount between 400 and 600 mm. Also, the bimodal rainfall regime over the Gulf of Guinea region occurs during the months from June to October, which represent the peaks of the long and short rainy seasons, respectively. In general. the total annual rainfall amounts over the Gulf of Guinea region range between 1500 and 2000 mm. Overall, these rainfall regimes follow the seasonal migration of the Intertropical Convergence Zone (ITCZ), which itself is linked to fluctuations in the trade wind system and the oceanic variables over the tropical Atlantic [52,53] and also associated with the northward penetration of the monsoon flux into the continent [53]. The influence of these mechanisms on the climatic zones depends largely on large-scale atmospheric circulations as well as continental and meteorological conditions [54–56].

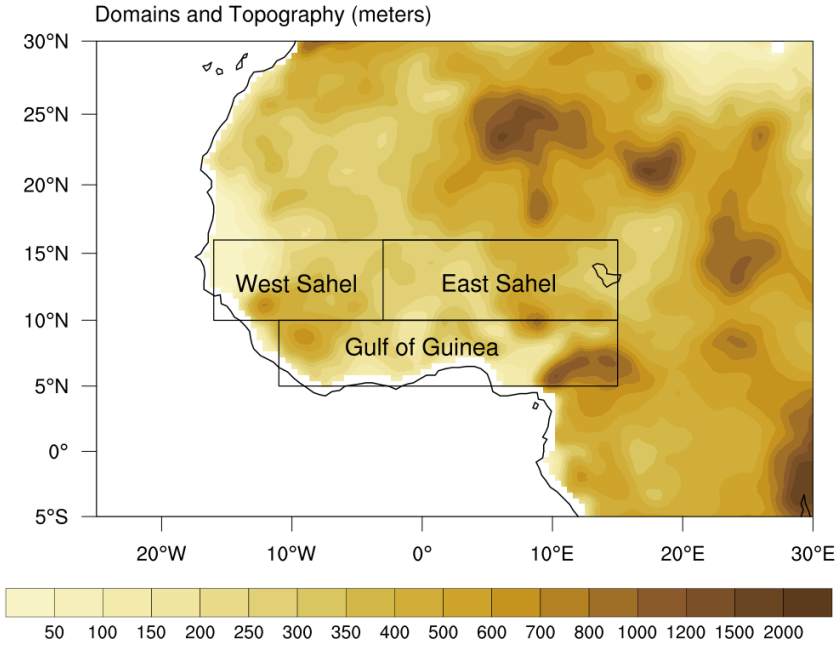

Figure 1. West African domain elevation in (m) including its three subregions (Western Sahel, Eastern Sahel, and Gulf of Guinea).

2.2. Data

In this study, we used daily precipitation and maximum temperature (see Table 1) data from an ensemble of four (04) Coordinated Regional Climate Downscaling Experiment (CORDEX) RCMs [41,57,58] available on the Earth System Grid Federation (ESGF) website (https://esg-dn1.nsc.liu.se/projects/esgf-liu/ (accessed on 31 March 2018)) at a resolution of 0.44° (~50 km) (see Table 2). CORDEX is a coordinated regional climate downscaling experiment program elaborated by an ensemble of research centers. It provides reliable and highly accurate climate change scenarios, enabling climate change impact studies at regional and local scales. It enables researchers to understand and analyze uncertainties in climate projections using regional climate models [41,57–59]. The data span the historical period of 1950–2005 and the future period of 2006–2100 under the scenarios of RCP4.5 and RCP8.5 [48,49,60]. These simulations are performed over a domain covering the whole of Africa. However, our domain of interest in this study was West Africa (see Figure 1). CORDEX simulations are useful in providing climate information using several meteorological parameters (i.e., temperature, rainfall, wind speed, etc.) and some extreme climate events (i.e., heatwaves, dry spells, etc.) over a specific region (i.e., Africa) at many time scales [37,60–62]. We also used the gridded gauge-based global daily precipitation and maximum temperature from Climate Prediction Center (CPC) observation data at a 0.5° (~50 km) resolution from 1979 to the present [63,64]. This dataset enabled us to evaluate the performance of the CORDEX simulations (Table 1).

Table 1. List of the different data (CORDEX simulations and CPC observation) with their resolutions and periods.

Simulations/Observation	Variables	Horizontal Resolution/Period	Scenarios
4 CORDEX [2] simulations 1 observation (CPC) [1]	Maximum temperature Precipitation	0.44° (≈50 Km) 1950–2005 2006–2100 1979–present	[3] RCP4.5 RCP8.5

[1] CPC: Climate Prediction Center; [1/2] CORDEX: Coordinated Downscaling Experiment; [3] RCP: Representative Concentration Pathway.

Table 2. The details of the CORDEX simulations composed of the RCMs and the GCMs used as boundary data.

[1] RCMs	[2] GCMs	Denotation
CCCma-CanRCM4	CanESM2	CCCMA
SMHI-RCA4	CNRM-CM5	RCA
DMI-HIRHAM5	EC-EARTH-r3	HIRHAM
CLMcom-CCLM4-8-17	MPI-ESM-LR	CCLM

[1] RCMs: regional climate models; [1/2] GCMs: global climate models/CCCMA: CCCma-CanRCM4 and CanESM2; RCA: SMHI-RCA4 and CNRM-CM5; HIRHAM: DMI-HIRHAM5 and EC-EARTH-r3; CCLM: CLMcom-CCLM4-8-17 and MPI-ESM-LR.

A detailed list of regional and global climate models used from CORDEX simulations are presented in Table 2. In this paper, we used a special denotation of the CORDEX simulations composed of RCMs and the GCMs in column 3 of Table 2.

2.3. Methods

2.3.1. Calculation of HWDI, CWD, and CDD Indices

In this study, we calculated three climate indicators defined by the Expert Team on Climate Change Detection and Indices (ETCCDI): the consecutive dry days (CDD), the consecutive wet days (CWD), and the heatwave duration index (HWDI). These indices describe the duration and number of dry and wet spells and heatwaves [65,66] (Table 3).

Table 3. ETCCDI indices used in this study [66,67].

Type of Index	Symbol	Expression	Unit
Precipitation	CDD [1]	CDD ($R_i < 1$ mm)	day
	CWD [2]	CWD ($R_i > 1$ mm)	day
Temperature	HWDI [3]	HWDI: $T_{Xi} > T_{X90}$, in an interval of at least three (03) consecutive days	day

[1] CDD: consecutive dry days; [2] CWD: consecutive wet days; [3] HWDI: heatwave duration index.

- CDD (consecutive dry days) is the greatest length of consecutive days when the precipitation amount is less than 1 mm/day. This is an indicator of dry spells (day) and drought. A further variable is the number of consecutive dry day periods of more than 5 days in a given time period.
- CWD (consecutive wet days) is the greatest length of consecutive days when the precipitation amount is greater than 1 mm/day. A further variable is the number of consecutive wet periods of more than 5 days in a given time period.
- HWDI (heatwave duration index) is the maximum period of at least three (or six) consecutive days where the daily maximum temperature exceeds the daily mean maximum temperature during the period of 1976–2005 + 5 °C [68]. A further derived variable is the number of heatwaves longer than or equal to three (or six) days. The daily mean maximum temperature during the period of 1976–2005 is calculated using a five-day window centered on each calendar day, considered as the climate reference period.

CDD, CWD, and HWDI indices are calculated on a grid for each simulation, then interpolated onto a common regular grid (0.5 × 0.5) degree of resolution using bilinear interpolation to enable the use of the multi-model ensemble (MME) approach. This approach allows the calculation of the mean of an ensemble of simulations to reduce existing uncertainties between them [39,42,69] using the following Equation (1):

$$MME = \frac{1}{N}\sum_{i=1}^{N} Simulation_i \quad (1)$$

where $Simulation_i$ represents each simulation and N represents the number of simulations.

2.3.2. An Evaluation of the Simulations' Ability to Represent the Indices

The ability of simulations to capture the variability in the annual cycle of CDD, CWD, and HWDI is assessed to better identify their respective strengths and weaknesses [70]. This technique is performed using the Taylor diagram [71,72] indicating three statistical quantities: the correlation coefficient (CC), the centered root-mean-square error (RMSE), and the amplitude of the variations represented by their standard deviation (SD). The aim is to identify the strengths and weakness of the different simulations through an easy and straightforward visual comparison [71,72]. In this study, the CORDEX simulations were compared to the unified gauge precipitation (CPC) in order to demonstrate their ability to reproduce the indices of CDD, CWD, and HWDI over the three subregions of West Africa for the historical period of 1976–2005.

2.3.3. Climate Change Signal

Climate change signal was evaluated using historical (1976–2005) and projected data under the RCP4.5 and RCP8.5 scenarios to investigate changes in the future. The changes were estimated as a percentage (%), with the historical mean period of 1976–2005 used as a reference. To this end, two future periods of thirty (30) years were considered, namely, the near-future period of 2031–2060 and the far-future period of 2071–2100, to obtain a more detailed description of the future climate, taking into account its evolution [73–76]. The climate change signal was evaluated using Equation (2) or Equation (3):

$$Climate\ change\ signal\ (\%) = \frac{projection - reference}{reference} * 100 \quad (2)$$

$$Climate\ change\ signal = projection - reference \quad (3)$$

where *projection* refers to the mean value of the variable (index) over a future period (2031–2060 or 2071–2100) and *reference* refers to the mean value of the variable (index) over the historical period (1976–2005).

3. Results and Discussion

3.1. Historical Seasonal Cycle of CDD, CWD, and HWDI Indices over the Different Subregions of West Africa

In this paragraph, the annual cycles of the different indices (CDD, CWD, and HWDI) over the three subregions (the Western Sahel, the Eastern Sahel, and the Gulf of Guinea) of the West African domain are intercompared using the observation data (CPC) and the four CORDEX simulations. This enables us to highlight the ability of the CORDEX simulations to outperform the annual cycle.

3.1.1. CDD Index and Its Number

Figure 2 presents the annual cycle of CDD and CDD number over the three subregions of West Africa. CDD and its number present the same variability during a year over the different subregions, as shown by CPC as well as the CORDEX simulations. The period from November to March is characterized by longer dry spells (about 30 days) and the occurrence of the maximum number of dry spells (about 2 days), while during the period of May–September, a shorter dry spell (about 10 days) is depicted, with a relatively smaller number of dry spells occurring over the whole West African region. During the period of May–September, considered the monsoon season in the Sahel regions (western and eastern), a lower occurrence of dry spells is indicated, while during the period of April–October, known as the monsoon season in the Gulf of Guinea region, there is a higher occurrence, as revealed by previous studies [52,53,59]. Overall, the annual cycle of CDD was well captured by the CORDEX simulations over all the three West African subregions, consistent with

results from other studies over West Africa [36,77] and over Central Africa [78]. The latter pointed out the accuracy of CORDEX simulations in capturing the annual cycle of CDD.

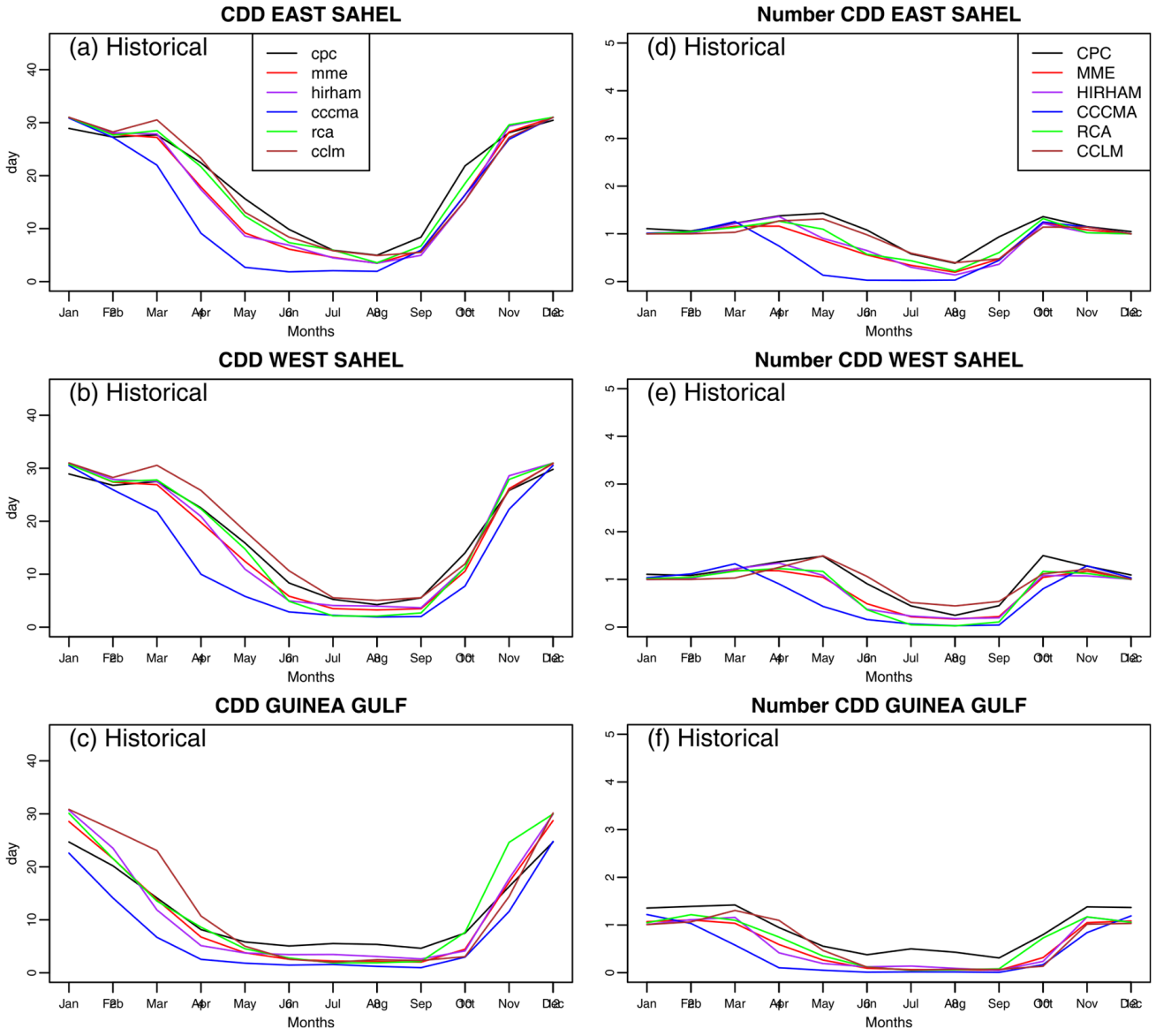

Figure 2. Seasonal cycle of CDD (**a**–**c**) and CDD number (**d**–**f**) over the different subregions for the observation data (CPC) and the CORDEX simulations.

3.1.2. CWD Index and CWD Number

The annual cycle variability in CWD and number of CWD over the three subregions of West Africa are presented in Figure 3. CWD and its number present bimodal variability during the year over the three subregions of West Africa, with an overestimation by the CORDEX simulations during the period from March to November. CCCMA overestimates CWD compared to other simulations, while HIRHAM simulates a similar pattern of CWD to other models compared to the CPC observation.

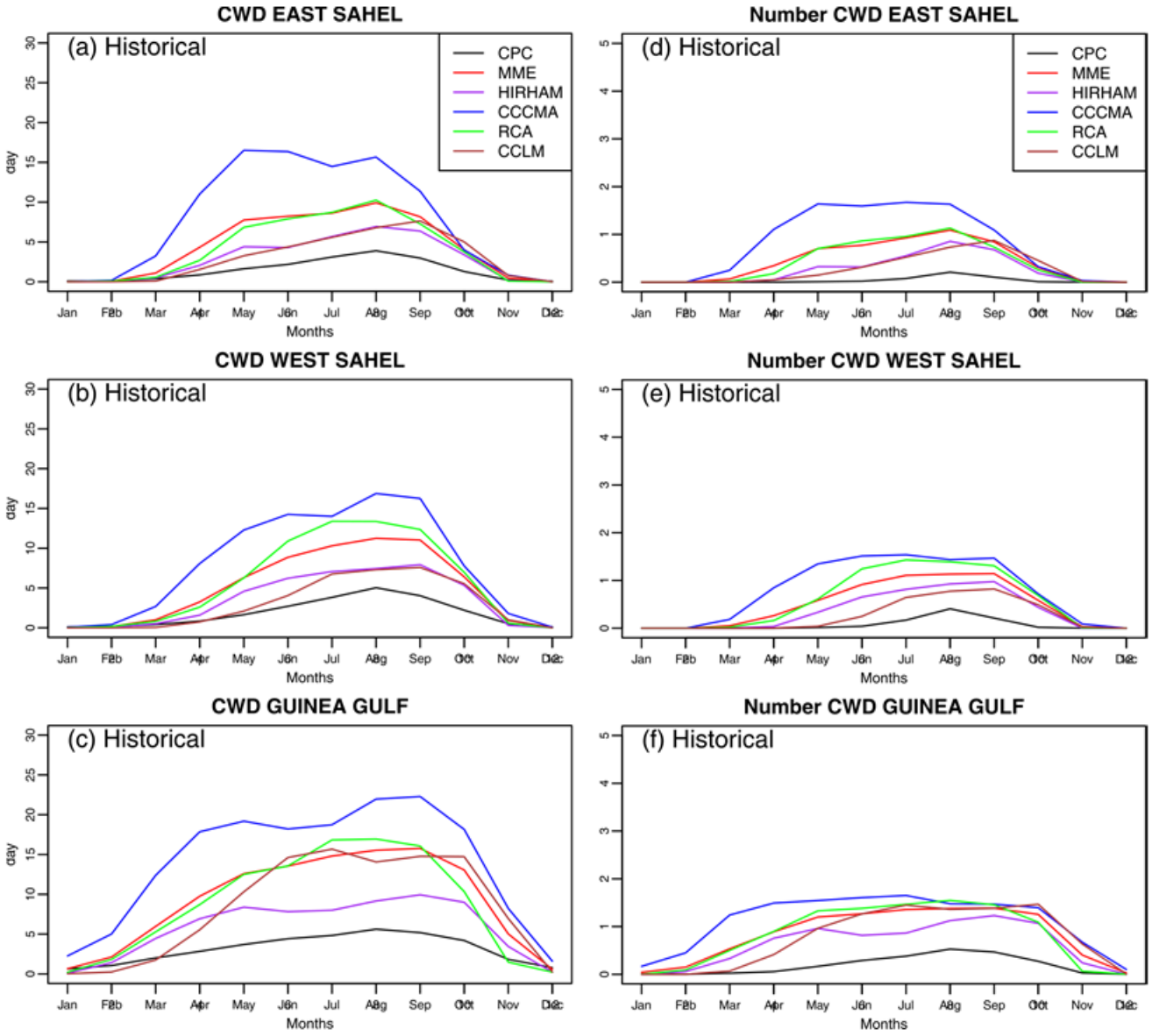

Figure 3. Same as Figure 2, but for CWD (**a**–**c**) and number of CWD (**d**–**f**).

3.1.3. HWDI and Number of HWDI

Figure 4 shows the variability in the annual cycle of HWDI and HWDI number for each West African subregion. HWDI and its number show the same seasonal cycle over each subregion. Over the Eastern Sahel, the seasonal variability in HWDI and its number exhibits three peaks in February, June and November. The Western Sahel presents two peaks in the months of March and May. In contrast, the observed seasonal cycle of HWDI and its number in the Gulf of Guinea indicates a marked peak in April. In summary, the seasonal variability in HWDI is well captured by the CORDEX simulations and their ensemble mean over the three subregions of West Africa, although some biases exist (Figure 4).

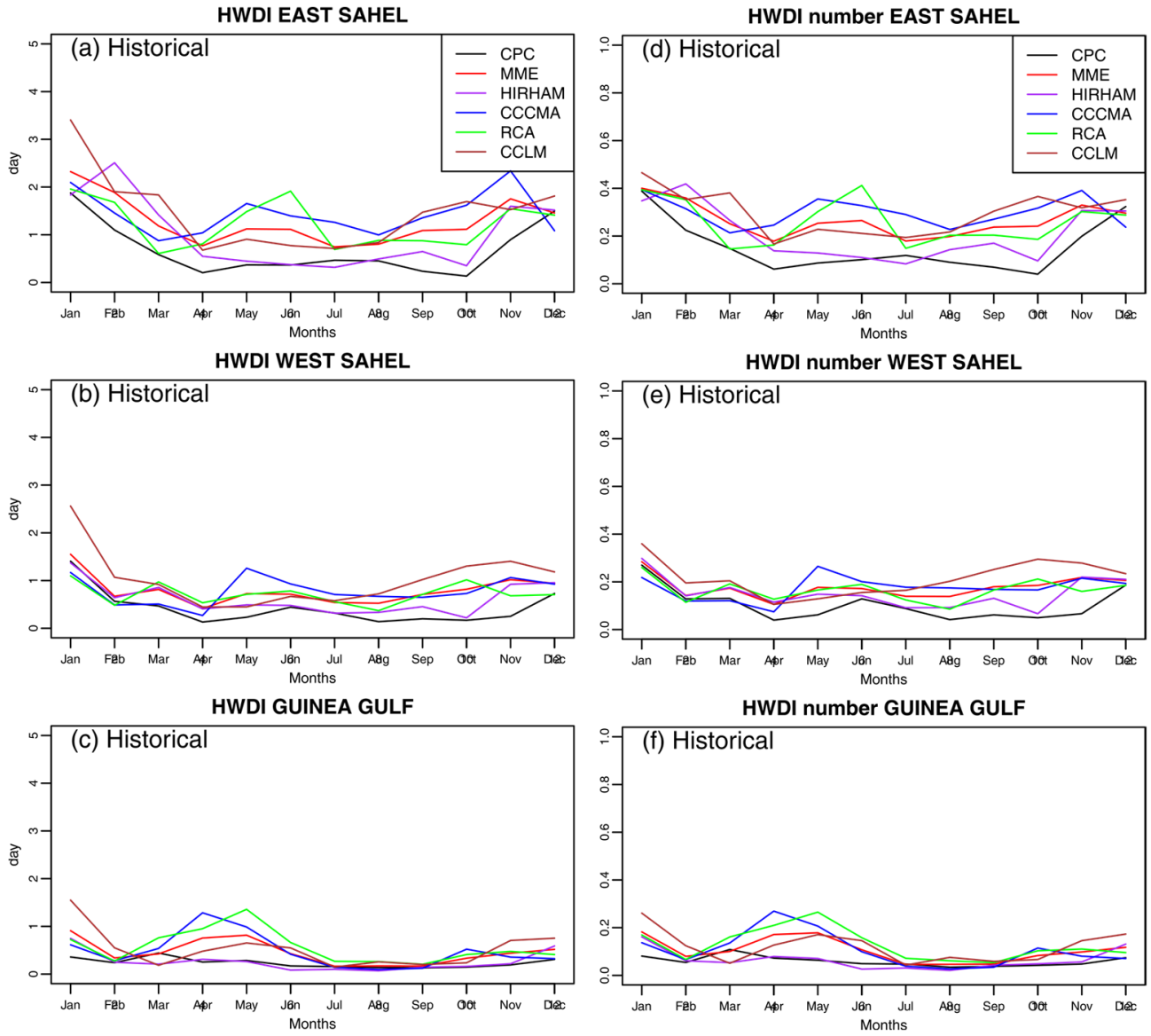

Figure 4. Same as Figures 2 and 3, but for HWDI (**a**–**c**) and number of HWDI (**d**–**f**).

3.2. Validation of the CORDEX Simulations of CDD, CWD, and HWDI over West African Subregions

Figures 5–7 show the performance of the CORDEX simulations in simulating the seasonal cycle of CDD, CWD, and HWDI over the three subregions of West Africa using the Taylor diagram during the period of 1979–2005 with respect to the CPC observation data used as a reference. The different CORDEX simulations are characterized by different-colored dots, as indicated in the legend (Figures 5–7). The green circles centered at the reference point represent the loci of constant RMS distance and the circles centered at the origin represent the loci of constant standard deviation. The correlation is represented as the cosine of the angle from the X-axis. The models with as much variance as the observation data, the largest correlation, and the smallest RMS error are considered the best performers in the Taylor diagram [79].

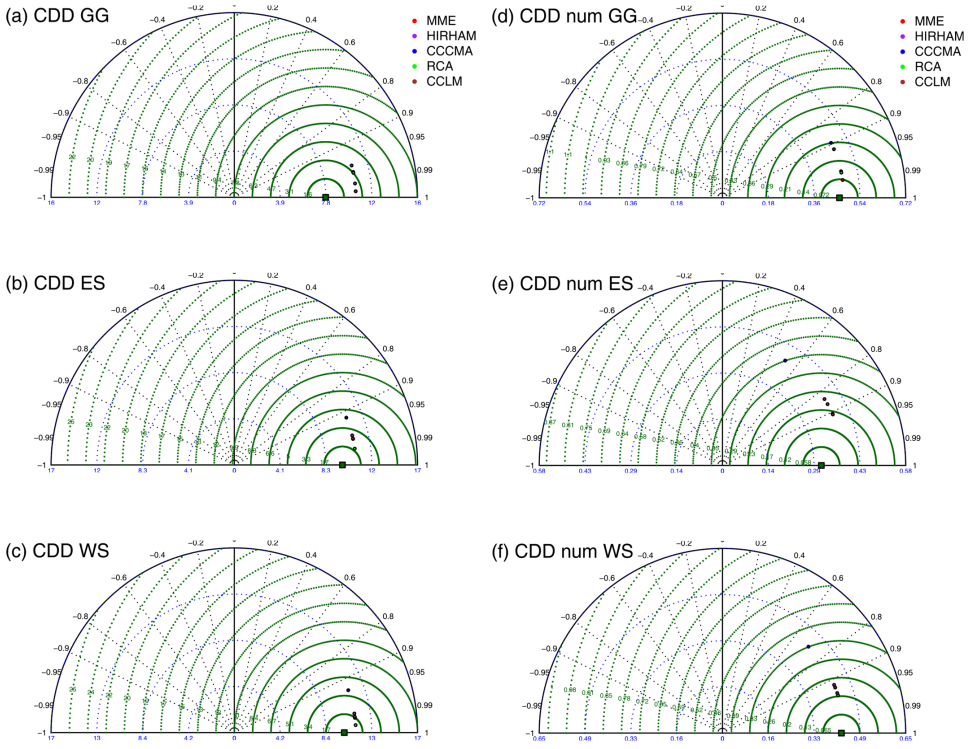

Figure 5. Taylor diagrams displaying a statistical comparison of CORDEX simulations and the CPC observation data for CDD and CDD number during the historical period (1976–2005) over Gulf of Guinea (GG; **a**,**d**), Eastern Sahel (ES; **b**,**e**), and Western Sahel (WS; **c**,**f**).

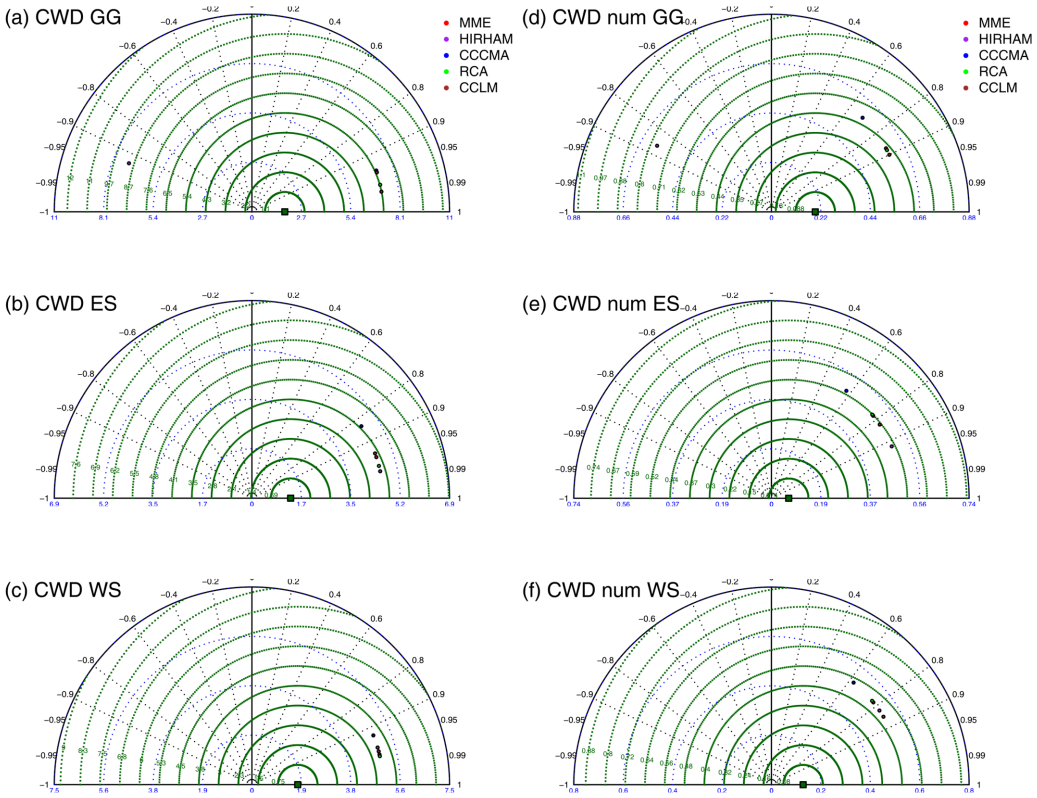

Figure 6. Same as Figure 5, but for CWD and CWD number.

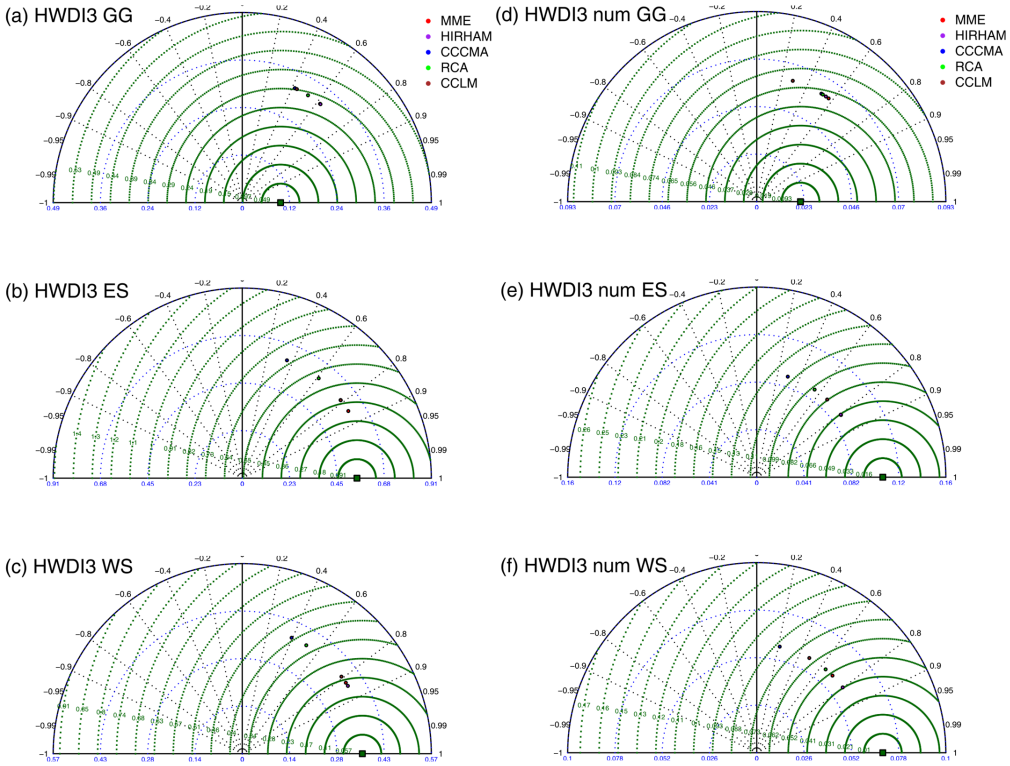

Figure 7. Same as Figures 5 and 6, but for HWDI and HWDI number.

3.2.1. CDD

Figure 5 shows the Taylor diagram of CDD and CDD number over the three subregions of West Africa. For the period of 1976–2005, all the CORDEX simulations overestimate the annual cycle of CDD and its number over West Africa with almost the same standard deviation but different root mean square differences (RMS). The CORDEX simulations have the correct standard deviation in capturing the CDD number over the Western Sahel and the Gulf of Guinea (Figure 5). In fact, the MME captures the amplitude of the CDD number over the Western Sahel and the Gulf of Guinea, with the RCA model being the best performer for CDD number over these subregions. These simulations indicate correlation coefficients of about 0.97 and 0.99, respectively; the CCLM simulation is the best performer over the Eastern Sahel with a 0.9 correlation coefficient. The Canadian simulation CCCMA shows the worst performance, with correlation coefficients of 0.9, 0.5, and 0.7 over the Gulf of Guinea, Eastern Sahel, and Western Sahel, respectively. Nevertheless, MME outperforms the others for CDD over the Gulf of Guinea subregion, with a correlation coefficient of more than 0.99, while RCA reproduces the CDD over the Eastern and Western Sahel reasonably well, with a correlation coefficient of more than 0.99. These results are in line with study [37].

3.2.2. CWD

The Taylor diagram of CWD and CWD number is presented in Figure 6. For each West African subregion, the CORDEX simulations almost present the same standard deviation (SD) and root mean square difference (RMS) with a correlation coefficient value greater than or equal to 0.6 for both CWD and its number, except for the HIRHAM model over the Gulf of Guinea, which indicates a negative correlation coefficient (Figure 6). Furthermore, the HIRHAM simulation outperforms the others for CWD and its number over the Eastern Sahel, while CCLM, MME, and RCA outperform the others for CWD and its number over the Gulf of Guinea and Western Sahel. Overall, the CORDEX simulations overestimate the CWD and its number over the whole West African region. These results are in agreement with study [59], which underlined that most of the CORDEX simulations overestimate

precipitation over Africa, although some biases exist based on the region, the season, and the evaluation metric.

3.2.3. HWDI

As with the CDD and CWD indices, the CORDEX simulations reproduce the HWDI and its number with the same standard deviation over West Africa. However, the amplitude of variation is well captured by the CORDEX simulations over the Eastern and Western Sahel, whereas an overestimation of the HWDI and its number is observed over the Gulf of Guinea subregion for the 1976–2005 period. In addition, MME agrees reasonably well with the CPC observation data in reproducing the HWDI over the Eastern Sahel and the HWDI number over the Gulf of Guinea, whereas the HIRHAM simulation outperforms the others in both the HWDI and its number over the Western Sahel, the HWDI alone over the Gulf of Guinea, and the HWDI number alone over the Eastern Sahel (Figure 7).

Overall, the correlation coefficient values between the CPC observation data and the different CORDEX simulations are summarized in Table 4.

Table 4. Correlation coefficients of CDD, CWD, and HWDI between the CPC observation data and the different CORDEX simulations over West African subregions.

			CDD		
	MME	**HIRHAM**	**CCCMA**	**RCA**	**CCLM**
GG	0.99	0.99	0.90	0.96	0.95
ES	0.96	0.96	0.91	0.995	0.94
WS	0.99	0.97	0.92	0.995	0.95
			CDD number		
GG	0.99	0.90	0.90	0.96	0.91
ES	0.81	0.85	0.5	0.95	0.90
WS	0.91	0.91	0.7	0.94	0.94
			CWD		
	MME	**HIRHAM**	**CCCMA**	**RCA**	**CCLM**
GG	0.99	−0.92	0.95	0.97	0.95
ES	0.95	0.97	0.82	0.97	0.95
WS	0.97	0.96	0.92	0.98	0.94
			CWD number		
GG	0.90	−0.75	0.70	0.88	0.87
ES	0.82	0.92	0.58	0.78	0.85
WS	0.85	0.82	0.62	0.78	0.78
			HWDI		
	MME	**HIRHAM**	**CCCMA**	**RCA**	**CCLM**
GG	0.42	0.62	0.40	0.50	0.80
ES	0.85	0.75	0.38	0.60	0.80
WS	0.84	0.85	0.40	0.50	0.78
			HWDI number		
GG	0.58	0.56	0.50	0.50	0.30
ES	0.65	0.80	0.30	0.58	0.65
WS	0.70	0.80	0.20	0.62	0.50

3.3. Projected Changes in the Annual Cycles of CDD, CWD, and HWDI Indices over West Africa

Future changes were evaluated with respect to the historical mean period (1979–2005) for each index over West Africa in order to determine the future evolution of these indices' characteristics from the present. The changes were evaluated over the near-future period (2031–2060) and far-future period (2071–2100) under the RCP4.5 and RCP8.5 scenarios.

3.3.1. Seasonal Changes in the HWDI

Figure 8 displays changes in the HWDI derived from the CORDEX simulations and their multi-model ensemble mean (red) during near- (2031–2060) and far- (2071–2100) future periods over West African subregions. A substantial increase in the HWDI is observed over the three subregions of West Africa during both periods. Under RCP8.5, the changes are more pronounced during the far future compared to the near future and under the RCP4.5 scenario. The projected changes in heatwaves may be related to possible changes in the dynamical features of the West African monsoon and the teleconnection with El Niño/ENSO in the context of global warming [80,81]. Especially in the coastal regions of West Africa, the moisture flux from the ocean associated with evapotranspiration over land increases the water vapor content entering the atmosphere, which could play a major role in heatwaves through an enhanced greenhouse effect [80,82]. However, the mechanism of heatwaves in Europe is different. In Europe, heatwaves are often associated with anticyclonic conditions, stronger sensible heat fluxes, and deeper boundary layers [80]. The fact that all CORDEX simulations indicate an increase in the HWDI suggests that the changes are robust [83,84]. These results suggest that heatwaves will be amplified in West Africa in future periods.

3.3.2. Seasonal Changes in CWD

Seasonal changes in CWD exhibit a general decrease from March to November over the Eastern and Western Sahel regions, with the CCCLM simulation showing the maximum decrease. In the Sahelian regions, almost no change is observed during the dry season ranging from December to February. However, the models project that the Gulf of Guinea region will experience a substantial decrease in CWD throughout the year, except for CCCLM, which projects an increase during September–December corresponding to the retreat of the monsoon in the region (Figure 9). The discrepancy shown by the CCCLM simulation during the September–December season over the Gulf of Guinea and the projected large changes in CWD over the Sahelian regions (eastern and western) are due to the convective scheme used by this model. Indeed, CCCLM employs the Tiedtke convective scheme [85], causing an overestimation of spells over the Sahel and flat terrains of the Guinea region [61].

3.3.3. Seasonal Changes in CDD

Figure 10 shows the projected changes in the annual cycle of CDD over the three subregions of West Africa during near- and far-future periods under the RCP4.5 and RCP8.5 scenarios. The simulations project a general increase in CDD during March–November over the Sahel, except RCA, which projects a decrease. In addition, CCCMA indicates a decrease in September during the near- and far-future periods under both RCP scenarios. Over the Gulf of Guinea region, discrepancies exist between the CORDEX simulations regarding the projected changes in CDD. Indeed, during the year, RCA and CCCLM show both a decrease and an increase in CDD, while other simulations clearly indicate only an increase, revealing some uncertainties in projected CDD. Overall, the multi-model ensemble (MME) mean shows an increase in CDD over West Africa but a slight decrease over the Gulf of Guinea in November–December during the late century under the RCP8.5 scenario. It is worth noting that the periods of CWD changes coincide with the periods of changes in CDD over the Sahelian regions (eastern and western). Our results are in line with the results of [78], which suggested that the increases in dry spells coupled with the decrease in wet spells and wet-day frequency could have strong consequences for seasonal rainfall onset, along with the total yearly rainfall amount over Central Africa. This implies that the increase in dry spells coupled with the decrease in wet spells could have negative effects on the environment and society. For instance, this situation could induce strong and severe drought and human discomfort in the future.

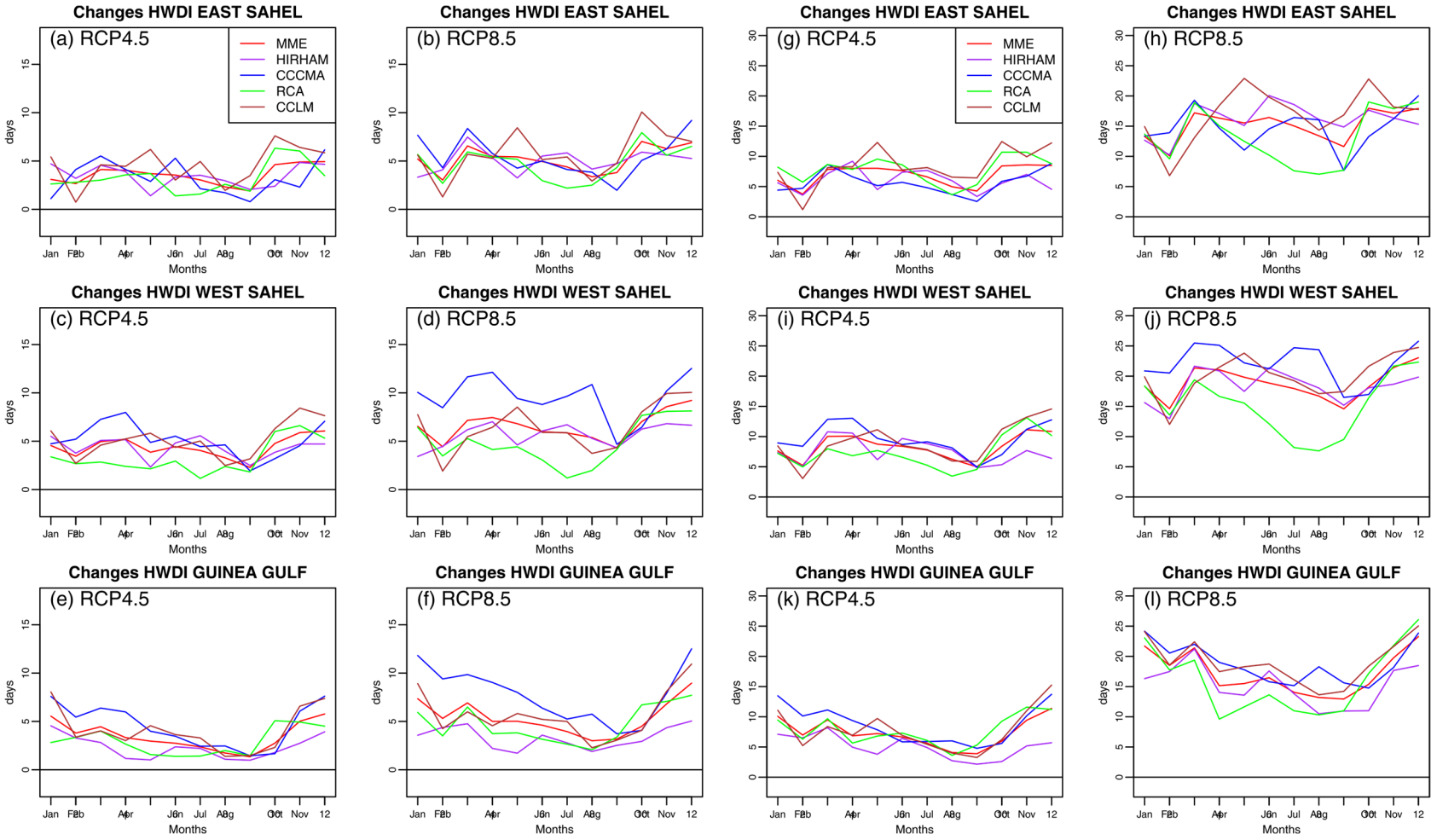

Figure 8. Projected changes in the seasonal cycle for HWDI during 2031–2060 (**a**–**f**) and 2071–2100 (**g**–**l**) relative to the baseline historical time period of 1976–2005 (horizontal line) under RCP4.5 and RCP8.5 scenarios.

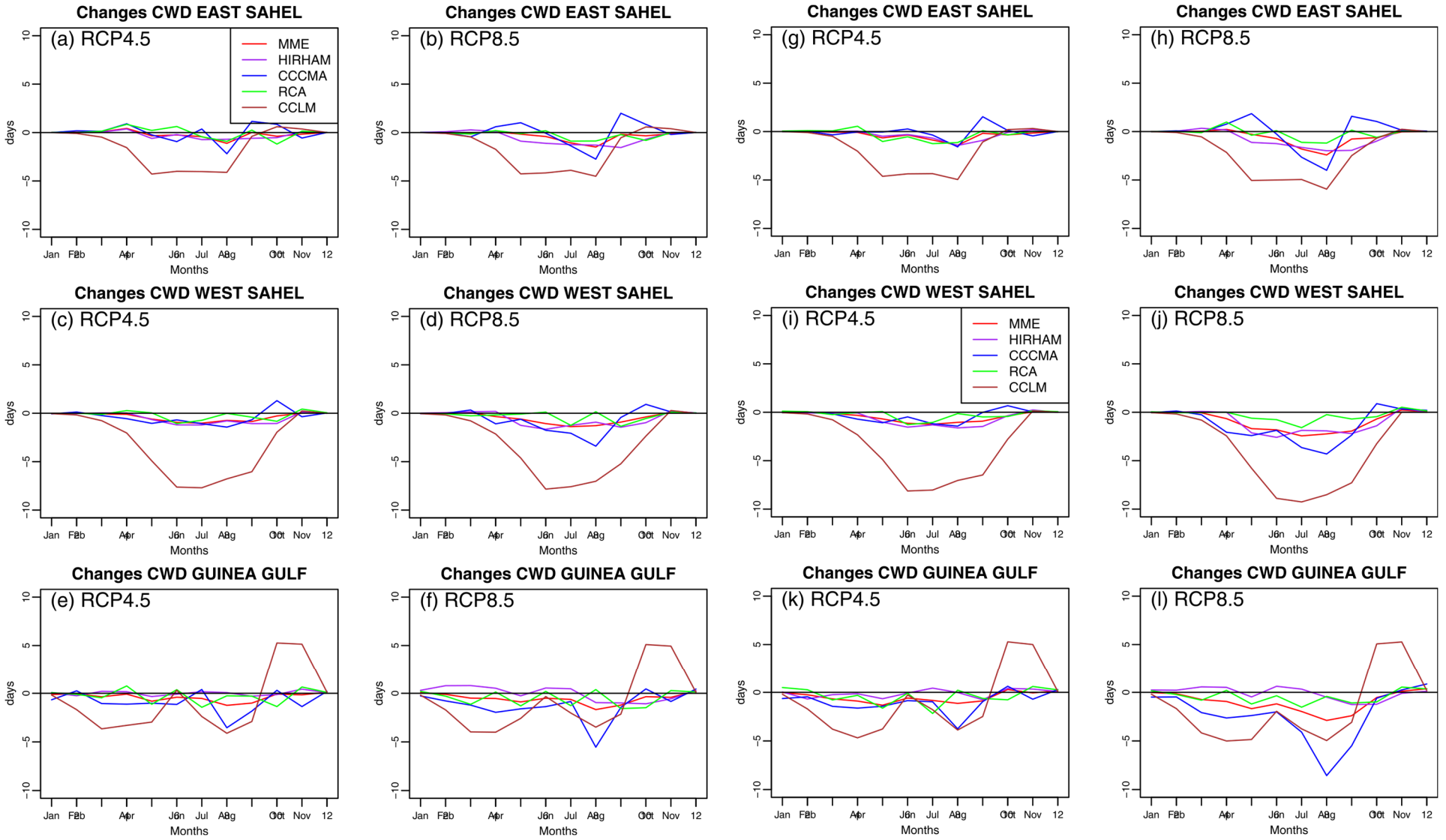

Figure 9. Same as Figure 8, but for CWD.

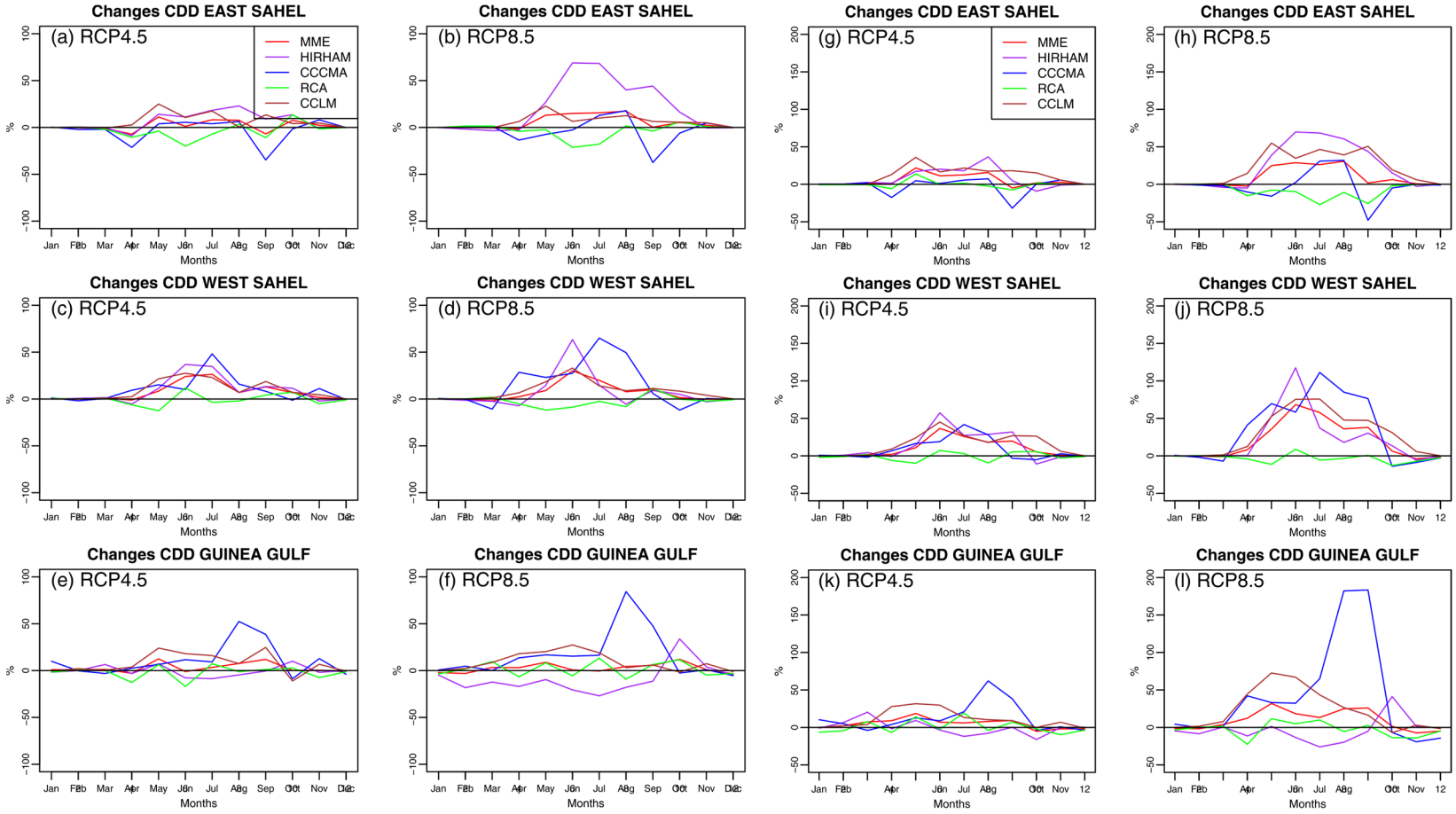

Figure 10. Same as Figures 8 and 9, but for CDD.

4. Summary and Conclusions

In this study, the projected changes in the seasonal cycles of heatwave and wet and dry spell indices were investigated over West Africa under RCP4.5 and RCP8.5's forcing scenarios. To this end, an ensemble of four CORDEX simulations and their ensemble mean with observation data (CPC) were used. Changes were calculated with respect to a reference period of 1976–2005 for near- (2031–2060) and far- (2071–2100) future periods. Firstly, the performance of the CORDEX simulations and their ensemble mean was evaluated in comparison to the CPC observation data in terms of the seasonal cycle of indices including heatwaves and wet and dry spells. The results of our analysis indicate that the CORDEX simulations realistically reproduce the seasonal cycle of heatwaves and wet and dry spells over the three defined subregions of West Africa (the Eastern Sahel, the Western Sahel, and the Gulf of Guinea) in the present climate, although some biases exist. In general, the latter are characterized by an underestimation of 30% for CDD and an overestimation of about 60% and 50% for CWD and HWDI, respectively. The different biases observed in individual CORDEX simulations are due to the use of different convective schemes for the parametrization of the simulations. In addition, CORDEX simulations and their ensemble means reproduce the different indices with the pattern variations of a similar order of magnitude reasonably well. On the one hand, individual simulations outperform their ensemble mean in terms of the variability in the indices. On the other hand, the projections indicate an increase of about 10 to 20 days in heatwave duration and number over the whole West African region under both forcing scenarios and in future periods. There is an increase (of about 80%) in dry spells, whereas there is a decrease (of about 40%) in wet spells observed over the West African region. However, the changes in dry and wet spells span the period from March to November over the Sahelian regions (the Eastern Sahel and Western Sahel), while over the Gulf of Guinea, the changes span the whole year, except a slight decrease in dry spells during the retreat phase of the monsoon (November–December) in the far future under RCP8.5. Almost all the CORDEX simulations agree on the projected signal of the seasonal cycles of the different indices, except CCCLM, which shows a discrepancy in the projected signal of CWD during the September–December season over the Gulf of Guinea. This suggests that the projected changes are robust. Finally, the period of increasing dry spells coincides with that of the decreasing wet spells over West Africa, indicating that West African countries will be at risk of severe drought, flooding, and heatwaves. Thus, governments and stakeholders must take action to suitably reduce greenhouse gas emissions in West Africa.

Author Contributions: Conceptualization, A.L.M.Y.; formal analysis, K.K. and D.T.T.; methodology, P.R.T.; software, A.M.L.F.; supervision, B.K.K. and A.D. (Adama Diawara); validation, A.D. (Arona Diedhiou); writing—original draft, F.Y. and M.B.S. All authors have read and agreed to the published version of the manuscript.

Funding: This research was funded by the Geophysical Station of Lamto.

Data Availability Statement: Data used in this study are available through this link: https://esg-dn1.nsc.liu.se/projects/esgf-liu/ (accessed on 31 March 2018).

Acknowledgments: The authors thank the anonymous reviewers and the editor for their constructive comments and suggestions, which helped improve the quality of the paper. The authors also thank the CORDEX program for the availability of their data and the Geophysical Station of Lamto for their technical support and facilities.

Conflicts of Interest: The authors declare no conflict of interest.

References

1. Boko, M.; Niang, I.; Nyong, A.; Vogel, C.; Githeko, A.; Medany, M.; Osman-Elasha, B.; Tabo, R.; Yanda, P. Africa. In *Climate Change 2007: Impacts, Adaptation and Vulnerability*; Contribution of Working Group II to the Fourth Assessment Report of the Intergovernmental Panel on Climate Change; Cambridge University Press: Cambridge, UK, 2007; pp. 433–467. Available online: https://cgspace.cgiar.org/handle/10568/17019 (accessed on 31 March 2018).
2. Niang, I.; Ruppel, O.C.; Abdrabo, M.A.; Essel, A.; Lennard, C.; Padgham, J. Africa. In *Climate Change 2014: Impacts, Adaptation, and Vulnerability. Part B: Regional Aspects*; Contribution of Working Group II to the Fifth Assessment Report of the Intergovernmental Panel on Climate Change; Barros, V.R., Field, D.J., Dokken, M.D., Mastrandrea, M.D., Mach, K.J., Billier, T.E., Eds.; Cambridge University Press: Cambridge, UK, 2014; pp. 1199–1265. Available online: https://ipcc-wg2.gov/AR5/images/uploads/WGIIAR5-Chap22_FINAL.pdf (accessed on 31 March 2018).
3. IPCC. Climate Change 2013: The Physical Science Basis. In *Contribution of Working Group I to the Fifth Assessment Report of the Intergovernmental Panel on Climate Change*; Cambridge University Press: Cambridge, UK, 2013; p. 1535.
4. Henseler, M.; Schumacher, I. The impact of weather on economic growth and its production factors. *Clim. Chang.* **2019**, *154*, 417–433. [CrossRef]
5. Charalampopoulos, I.; Nastos, P.T.; Didaskalou, E. Human Thermal Conditions and North Europeans' Web Searching Behavior (Google Trends) on Mediterranean Touristic Destinations. *Urban Sci.* **2017**, *1*, 8. [CrossRef]
6. Schmitt, L.H.M.; Graham, H.M.; White, P.C.L. Economic Evaluations of the Health Impacts of Weather-Related Extreme Events: A Scoping Review. *Int. J. Environ. Res. Public Health* **2016**, *13*, 1105. [CrossRef]
7. Felbermayr, G.; Gröschl, J.; Sanders, M.; Schippers, V.; Steinwachs, T. The economic impact of weather anomalies. *World Dev.* **2022**, *151*, 20. [CrossRef]
8. Charalampopoulos, I.; Droulia, F. The Agro-Meteorological Caused Famines as an Evolutionary Factor in the Formation of Civilisation and History: Representative Cases in Europe. *Climate* **2021**, *14*, 5. [CrossRef]
9. Langue, C.; Gacial, N.; Lavaysse, C.; Vrac, M.; Flamant, C. Heat wave monitoring over West African cities: Uncertainties, characterization and recent trends. *Nat. Hazards Earth Syst. Sci.* **2023**, *23*, 1313–1333. [CrossRef]
10. Wang, P.; Tang, J.; Sun, X.; Liu, J.; Juan, F. Spatiotemporal characteristics of heat waves over China in regional climate simulations within the CORDEX-EA project. *Clim. Dyn.* **2019**, *52*, 799–818. [CrossRef]
11. Tanarhte, M.; Hadjinicolaou, P.; Lelieveld, J. Heat wave characteristics in the eastern Mediterranean and Middle East using extreme value theory. *Clim. Res.* **2015**, *63*, 99–113. [CrossRef]
12. Wang, H.; Gao, Y.; Wang, Y.; Sheng, L. Arctic Sea ice modulation of summertime heatwaves over western North America in recent decades. *Environ. Res. Lett.* **2022**, *17*, 9. [CrossRef]
13. Barriopedro, D.; Fischer, E.M.; Luterbacher, J.; Trigo, R.M.; Garcia-Herrera, R. The Hot Summer of 2010: Redrawing the Temperature Record Map of Europe. *Science* **2011**, *332*, 220–224. Available online: www.sciencemag.org (accessed on 31 March 2018).
14. Guerreiro, S.B.; Dawson, R.J.; Kilsby, C.; Lewis, E.; Ford, A. Future heat-waves, droughts and floods in 571 European cities. *Environ. Res. Lett.* **2018**, *13*, 10. [CrossRef]
15. Russo, S.; Sillmann, J.; Fischer, E.M. Top ten European heatwaves since 1950 and their occurrence in the coming decades. *Environ. Res. Lett.* **2015**, *10*, 15. [CrossRef]
16. Bessemoulin, P.; Bourdette, N.; Courtier, P.; Manach, J. La canicule d'Août 2003 en France et en Europe. *Météorologie* **2004**, *46*, 25–33. [CrossRef]
17. Poumadère, M.; Mays, C.; Le Mer, S.; Blong, R. The 2003 Heat Wave in France: Dangerous Climate Change Here and Now. *Risk Anal.* **2005**, *25*, 1483–1494. [CrossRef] [PubMed]
18. Matsueda, M. Predictability of Euro-Russian blocking in summer of 2010. *Geophys. Res. Lett.* **2011**, *38*, 1–6. [CrossRef]
19. Russo, S.; Marchese, A.F.; Sillmann, J.; Immé, G. When will unusual heat waves become normal in a warming Africa? *Environ. Res. Lett.* **2016**, *11*, 375–380. [CrossRef]
20. Rome, S.; Caniaux, G.; Ringard, J.; Dieppois, B.; Diedhiou, A. Identification de tendances récentes et ruptures d' homogénéité des températures: Exemple en Afrique de l'Ouest et sur le Golfe de Guinée. In Proceedings of the XXVIII Colloquium of the International Association of Climatology, Liège, Belgium, 1–4 July 2015; pp. 591–596.
21. Ringard, J.; Dieppois, B.; Rome, S.; Diedhiou, A.; Pellarin, T.; Konaré, A.; Dje, B.K.; Katiellou, G.L.; Sanda, I.S. The intensification of thermal extremes in west Africa. *Glob. Planet Chang.* **2016**, *139*, 66–77. [CrossRef]
22. Sylla, M.B.; Faye, A.; Giorgi, F.; Diedhiou, A.; Kunstmann, H. Projected Heat Stress Under 1.5 °C and 2 °C Global Warming Scenarios Creates Unprecedented Discomfort for Humans in West Africa. *Earth's Future* **2018**, *6*, 16. [CrossRef]
23. Jahn, M. Economics of extreme weather events: Terminology and regional impact models. *Weather Clim. Extrem.* **2015**, *10*, 29–39. [CrossRef]
24. Stefanon, M.; D'Andrea, F.; Drobinski, P. Heatwave classification over Europe and the Mediterranean region. *Environ. Res. Lett.* **2012**, *7*, 9. [CrossRef]
25. IPCC. Summary for Policymakers. In *Managing the Risks of Extreme Events and Disasters to Advance Climate Change Adaptation*; Cambridge University Press: Cambridge, UK, 2012. Available online: http://ebooks.cambridge.org/ref/id/CBO9781139177245 (accessed on 31 March 2018).

26. Perkins-Kirkpatrick, S.E.; Gibson, P.B. Changes in regional heatwave characteristics as a function of increasing global temperature. *Sci. Rep.* **2017**, *7*, 12. [CrossRef] [PubMed]
27. Yapo, A.L.M. Impacts du Changement Climatique sur la Fréquence et l'Intensité des Evènements Extrêmes en Côte d'Ivoire. Ph.D. Thesis, University Félix Houphouet-Boigny, Abidjan, Côte d'Ivoire, 2021; p. 208.
28. Steadman, R.G. The Assessment of Sultriness. Part I: A Temperature-Humidity Index Based on Human Physiology and Clothing Science. *J. Appl. Meteorol. Clim.* **1979**, *18*, 861–873. [CrossRef]
29. Steadman, R.G. The assessment of sultriness. Part II: Effects of wind, extra radiation and barometric pressure on apparent temperature. *J. Appl. Meteorol.* **1979**, *18*, 874–885. [CrossRef]
30. Wang, C.; Zheng, J.; Lin, W.; Wang, Y. Unprecedented Heatwave in Western North America during Late June of 2021: Roles of Atmospheric Circulation and Global Warming. *Adv. Atmos. Sci.* **2023**, *40*, 14–28. [CrossRef]
31. Wehner, M.; Castillo, F.; Stone, D. The impact of moisture and temperature on human health in heat waves. In *Oxford Research Encyclopedia of Natural Hazard Science*; Oxford University Press: Oxford, UK, 2017.
32. Engdaw, M.M.; Ballinger, A.P.; Hegerl, G.C.; Steiner, A.K. Changes in temperature and heat waves over Africa using observational and reanalysis data sets. *Int. J. Climatol.* **2021**, *42*, 1165–1180. [CrossRef]
33. Oueslati, B.; Pohl, B.; Moron, V.; Rome, S.; Janicot, S. Characterization of Heat Waves in the Sahel and Associated Physical Mechanisms. *J. Clim.* **2017**, *30*, 3095–3115. [CrossRef]
34. Shafiei Shiva, J.; Chandler, D.G.; Kunkel, K.E. Localized Changes in Heat Wave Properties Across the United States. *Earth's Future* **2019**, *7*, 300–319. [CrossRef]
35. Camara, M.; Diedhiou, A.; Sow, B.A.; Diallo, M.D.; Diatta, S.; Mbaye, I.; Diallo, I. Analyse de la pluie simulée par les modèles climatiques régionaux de CORDEX en Afrique de l'Ouest. *Sécheresse* **2013**, *24*, 14–28.
36. Gbobaniyi, E.; Sarr, A.; Sylla, M.B.; Diallo, I.; Lennard, C.; Dosio, A.; Dhiediou, A.; Kamga, A.; Klutse, N.A.; Hewitson, B.; et al. Climatology, annual cycle and interannual variability of precipitation and temperature in CORDEX simulations over West Africa. *Int. J. Climatol.* **2013**, *34*, 2241–2257. [CrossRef]
37. Klutse, N.A.B.; Sylla, M.B.; Diallo, I.; Sarr, A.; Dosio, A.; Diedhiou, A.; Kamga, A.; Lamptey, B.; Ali, A.; Owusu, K. Daily characteristics of West African summer monsoon precipitation in CORDEX simulations. *Theor. Appl. Climatol.* **2015**, *123*, 369–386. [CrossRef]
38. Sarr, A.B.; Camara, M.; Diba, I. Spatial Distribution of Cordex Regional Climate Models Biases over West Africa. *Int. J. Geosci.* **2015**, *6*, 1018–1031. [CrossRef]
39. Nikiema, P.M.; Sylla, M.B.; Ogunjobi, K.; Kebe, I.; Gibba, P.; Giorgi, F. Multi-model CMIP5 and CORDEX simulations of historical summer temperature and precipitation variabilities over West Africa. *Int. J. Climatol.* **2016**, *37*, 2438–2450. [CrossRef]
40. Gibba, P.; Sylla, M.B.; Okogbue, E.C.; Gaye, A.T.; Nikiema, M.; Kebe, I. State-of-the-art climate modeling of extreme precipitation over Africa: Analysis of CORDEX added-value over CMIP5. *Theor. Appl. Climatol.* **2018**, *137*, 1041–1057. [CrossRef]
41. Giorgi, F.; Gutowski, W.J. Coordinated Experiments for Projections of Regional Climate Change. *Curr. Clim. Chang. Rep.* **2016**, *2*, 202–210. [CrossRef]
42. Diallo, I.; Sylla, M.B.; Giorgi, F.; Gaye, A.T.; Camara, M. Multimodel GCM-RCM ensemble-based projections of temperature and precipitation over West Africa for the Early 21st Century. *Int. J. Geophys.* **2012**, *2012*, 972896. [CrossRef]
43. Sylla, M.B.; Gaye, A.T.; Jenkins, G.S. On the fine-scale topography regulating changes in atmospheric hydrological cycle and extreme rainfall over West Africa in a regional climate model projections. *Int. J. Geophys.* **2012**, *2012*, 981649. [CrossRef]
44. Tall, M.; Sylla, M.B.; Diallo, I.; Pal, J.S.; Faye, A.; Mbaye, M.L.; Gaye, A.T. Projected impact of climate change in the hydroclimatology of Senegal with a focus over the Lake of Guiers for the twenty-first century. *Theor. Appl. Climatol.* **2016**, *129*, 655–665. [CrossRef]
45. Klutse, N.A.B.; Ajayi, V.O.; Gbobaniyi, E.O.; Egbebiyi, T.S.; Kouadio, K.; Nkrumah, F.; Quagraine, K.A.; Olusegun, C.; Diasso, U.; Abiodun, R.I.; et al. Potential impact of 1.5 °C and 2 °C global warming on consecutive dry and wet days over West Africa. *Environ. Res. Lett.* **2018**, *13*, 7. Available online: http://iopscience.iop.org/article/10.1088/1748-9326/aab37b (accessed on 31 March 2018). [CrossRef]
46. Yapo, A.L.M.; Diawara, A.; Kouassi, B.; Yoroba, F.; Sylla, M.B.; Kouadio, K.; Tieomoko, D.T.; Kone, D.I.; Akobe, E.Y.; Yao, K.P. Twenty-First Century Projected Changes in Extreme Temperature over Côte d' Ivoire (West Africa). *Int. J. Geophys.* **2019**, *2019*, 19. [CrossRef]
47. Yapo, A.L.M.; Diawara, A.; Kouassi, B.K.; Yoroba, F.; Sylla, M.B.; Kouadio, K.; Tiemoko, D.T.; Kone, D.I.; Akobe, E.Y.; Yao, K.P. Projected changes in extreme precipitation intensity and dry spell length in Côte d'Ivoire under future climates. *Theor. Appl. Climatol.* **2020**, *19*, 871–889. [CrossRef]
48. Van Vuuren, D.P. Representative Concentration Pathways: An overview. *Clim. Chang.* **2011**, *109*, 5–31. [CrossRef]
49. Moss, R.H.; Edmonds, J.A.; Hibbard, K.A.; Manning, M.R.; Rose, S.K.; Van Vuuren, D.P.; Carter, T.R.; Emori, S.; Kainuma, M.; Kram, T.; et al. The next generation of scenarios for climate change research and assessment. *Nature* **2010**, *463*, 747–756. [CrossRef] [PubMed]
50. Sylla, M.B.; Diallo, I.; Pal, J.S. West African Monsoon in State-of-the-Science Regional Climate Models. Climate Variability—Regional and Thematic Patterns. 2013. Available online: http://www.intechopen.com/books/climate-variability-regional-and-thematic-patterns/west-african-monsoon-in-state-of-the-science-regional-climate-models (accessed on 31 March 2018).

51. Nicholson, S.E.; Palao, I.M. A reevaluation of rainfall variability in the Sahel. Part, I. Characteristics of rainfall fluctuations. *Int. J. Climatol.* **1993**, *13*, 371–389. [CrossRef]
52. Ward, N. Diagnosis and short lead time prediction of summer rainfall in tropical North Africa at interannual and multidecadal timescales. *J. Clim.* **1998**, *12*, 3167–3191. [CrossRef]
53. Sultan, B.; Janicot, S.; Drobinski, P. Characterization of the diurnal cycle of the West African Monsoon around the Monsoon Onset. *J. Clim.* **2007**, *20*, 4014–4032. [CrossRef]
54. Fontaine, B.; Janicot, S. Wind-field coherence and its variations over west Africa. *J. Clim.* **1992**, *5*, 512–524. [CrossRef]
55. Diawara, A.; Yoroba, F.; Kouadio, K.Y.; Kouassi, K.B.; Assamoi, E.M.; Diedhiou, A.; Assamoi, P. Climate Variability in the Sudano-Guinean Transition Area and Its Impact on Vegetation: The Case of the Lamto Region in Côte D 'Ivoire. *Adv. Meteorol.* **2014**, *2014*, 831414. [CrossRef]
56. Ta, S.; Kouadio, K.Y.; Ali, K.E.; Toualy, E.; Aman, A.; Yoroba, F. West Africa Extreme Rainfall Events and Large-Scale Ocean Surface and Atmospheric Conditions in the Tropical Atlantic. *Adv. Meteorol.* **2016**, *2016*, 1940456. [CrossRef]
57. Giorgi, F.; Jones, C.; Asrar, G.R. Addressing climate information needs at the regional level: The CORDEX framework. *WMO Bull.* **2009**, *58*, 175–183.
58. Giorgi, F.; Gutowski, W.J. Regional Dynamical Downscaling and the CORDEX Initiative. *Annu. Rev. Environ. Resour.* **2015**, *40*, 24. [CrossRef]
59. Nikulin, G.; Jones, C.; Giorgi, F.; Asrar, G.; Büchner, M.; Cerezo-Mota, R.; Deque, M.; Fernandez, J.; Hansler, A.; Meijgaard, E. Precipitation climatology in an ensemble of CORDEX-Africa regional climate simulations. *J. Clim.* **2012**, *25*, 6057–6078. [CrossRef]
60. Riede, J.O.; Posada, R.; Fink, A.H.; Kaspar, F. Chapter 2—What's on the 5th IPCC Report for West Africa. In *Adaptation to Climate Change and Variability in Rural West Africa*; Springer: Berlin/Heidelberg, Germany, 2016; pp. 7–24.
61. Dosio, A.; Panitz, H.J. Climate change projections for CORDEX-Africa with COSMO-CLM regional climate model and differences with the driving global climate models. *Clim. Dyn.* **2016**, *46*, 1599–1625. [CrossRef]
62. Pinto, I.; Lennard, C.; Tadross, M.; Hewitson, B.; Dosio, A.; Nikulin, G.; Panitz, H.J.; Shongwe, M.E. Evaluation and projections of extreme precipitation over southern Africa from two CORDEX models. *Clim. Change* **2016**, *135*, 14. [CrossRef]
63. Chen, M.; Shi, W.; Xie, P.; Silva, V.B.S.; Kousky, V.E.; Wayne, H.R.; Higgins, R.; Janowiak, J.E. Assessing objective techniques for gauge-based analyses of global daily precipitation. *J. Geophys. Res.* **2008**, *113*, D04110. [CrossRef]
64. Diaconescu, E.P.; Gachon, P.; Scinocca, J.; Laprise, R. Evaluation of daily precipitation statistics and monsoon onset/retreat over western Sahel in multiple data sets. *Clim. Dyn.* **2015**, *45*, 1325–1354. [CrossRef]
65. Klein, T.A.M.G.; Peterson, T.C.; Quadir, D.A.; Dorji, S.; Zou, X.; Tang, H.; Santhosh, K.; Joshi, U.R.; Jaswal, A.K.; Kolli, R.K.; et al. Changes in daily temperature and precipitation extremes in central and south Asia. *J. Geophys. Res.* **2006**, *111*, D16105. [CrossRef]
66. Klein, T.A.M.G.; Zwiers, F.W.; Zhang, X. Guidelines on Analysis of extremes in a changing climate in support of informed decisions for adaptation. *World Meteorol. Organ.* **2009**, *72*, 56.
67. Zhang, X.; Alexander, L.; Hegerl, G.C.; Jones, P.; Tank, A.K.; Peterson, T.C.; Trewin, B.; Zwiers, F.W. Indices for monitoring changes in extremes based on daily temperature and precipitation data. *Wiley Interdiscip. Rev. Clim. Chang.* **2011**, *6*, 851–870. [CrossRef]
68. Perkins, S.E. A review on the scientific understanding of heatwaves—Their measurement, driving mechanisms, and changes at the global scale. *Atmos. Res.* **2015**, *164*, 242–267. [CrossRef]
69. Sylla, M.B.; Gaye, A.; Jenkins, G.; Pal, J.S.; Giorgi, F. Consistency of projected drought over the Sahel with changes in the monsoon circulation and extremes in a regional climate model. *J. Geophys. Res.* **2010**, *115*, 10. [CrossRef]
70. Haensler, A.; Jacob, D.; Kabat, P.; Ludwig, F. Assessment of projected climate change signals over central Africa based on a multitude of global and regional climate projections. Climate Change Scenarios for the Congo Basin. 2013, pp. 11–42. Available online: www.climate-service-center.de/imperia/md/content/csc/csc-report11_optimized.pdf (accessed on 31 March 2018).
71. Kalognomou, E.A.; Lennard, C.; Shongwe, M.; Pinto, I.; Favre, A.; Kent, M.; Hewitson, B.; Dosio, A.; Nikulin, G.; Panitz, H.J.; et al. A Diagnostic evaluation of precipitation in CORDEX models over Southern Africa. *J. Clim.* **2013**, *26*, 9477–9506. [CrossRef]
72. Taylor, K.E. Summarizing multiple aspects of model performance in a single diagram. *J. Geophys. Res.* **2001**, *106*, 7183–7192. [CrossRef]
73. Taylor, K.E. Taylor Diagram Primer. Work Paper. pp. 1–4. 2005. Available online: https://bigladdersoftware.com/projects/elements/ (accessed on 31 March 2018).
74. Diallo, I.; Giorgi, F.; Deme, A.; Tall, M.; Mariotti, L.; Gaye, A.T. Projected changes of summer monsoon extremes and hydroclimatic regimes over West Africa for the twenty-first century. *Clim. Dyn.* **2016**, *47*, 3931–3954. [CrossRef]
75. Sylla, M.B.; Nikiema, P.M.; Gibba, P.; Kebe, I.; Ama, N.; Klutse, B. Climate Change over West Africa: Recent Trends and Future Projections. 2016. pp. 25–40. Available online: http://link.springer.com/10.1007/978-3-319-31499-0 (accessed on 31 March 2018).
76. Abiodun, B.J.; Adegoke, J.; Abatan, A.A.; Ibe, C.A.; Egbebiyi, T.S.; Engelbrecht, F.; Pinto, I. Potential impacts of climate change on extreme precipitation over four African coastal cities. *Clim. Chang.* **2017**, *143*, 399–413. [CrossRef]
77. Sarr, A.B.; Camara, M. Evolution Des Indices Pluviométriques Extrêmes Par L'analyse De Modèles Climatiques Régionaux Du Programme CORDEX: Les Projections Climatiques Sur Le Sénégal. *Eur. Sci. J.* **2017**, *13*, 206–222. Available online: http://eujournal.org/index.php/esj/article/view/9521/9029 (accessed on 31 March 2018). [CrossRef]
78. Sylla, M.B.; Giorgi, F.; Pal, J.S.; Gibba, P.; Kebe, I.; Nikiema, M. Projected changes in the annual cycle of high-intensity precipitation events over West Africa for the late twenty-first century. *J. Clim.* **2015**, *28*, 6475–6488. [CrossRef]

79. Fotso-Nguemo, T.C.; Diallo, I.; Diakhaté, M.; Vondou, D.A.; Mbaye, M.L.; Haensler, A.; Haye, A.T.; Tchawouau, C. Projected changes in the seasonal cycle of extreme rainfall events from CORDEX simulations over Central Africa. *Clim. Chang.* **2019**, *19*, 339–357. [CrossRef]
80. Chaturvedi, R.K.; Joshi, J.; Jayaraman, M.; Bala, G.; Ravindranath, N.H. Multi-model climate change projections for India under representative concentration pathways. *Curr. Sci.* **2012**, *103*, 791–802.
81. Barbier, J. Extrêmes Climatiques: Les Vagues de Chaleur au Printemps Sahélien. Ph.D. Thesis, l'Université Toulouse, Toulouse, France, 2017; p. 160.
82. Sillmann, J.; Thorarinsdottir, T.; Keenlyside, N.; Schaller, N.; Alexander, L.V.; Hegerl, G.; Seneviratne, S.I.; Vautard, R.; Zhang, X.; Zwiers, F.W. Understanding, modeling and predicting weather and climate extremes: Challenges and opportunities. *Weather Clim. Extrem.* **2017**, *18*, 65–74. [CrossRef]
83. Sillmann, J.; Kharin, V.V.; Zwiers, F.W.; Zhang, X.; Bronaugh, D. Climate extremes indices in the CMIP5 multimodel ensemble: Part 2. Future climate projections. *J. Geophys. Res. Atmos.* **2013**, *118*, 2473–2493. [CrossRef]
84. GIEC. *Résumé à l'Intention des Décideurs. Bilan 2007 des Chang Clim Impacts, Adapt Vulnérabilité Contribut du Groupe Trav II au Quatrième Rapp d'Evaluation Rapp du Groupe d'Experts Intergouv sur l'Evolution du Clim*; Parry, M.L., Canzani, O.F., Eds.; Cambridge University Press: Cambridge, UK, 2007.
85. Tiedtke, M. A comprehensive mass flux scheme for cumulus parameterization in largescale models. *Mon. Weather Rev.* **1989**, *117*, 1779–1800. [CrossRef]